WARSAW UNIVERSITY OF TECHNOLOGY Index 351733
FACULTY OF CIVIL ENGINEERING
COMMITTEE FOR CIVIL AND WATER ENGINEERING
POLISH ACADEMY OF SCIENCES ISSN 1230-2945
DOI: 10.24425/ace.2025.155120
ARCHIVES OF CIVIL ENGINEERING
Vol. LXXI ISSUE 3 2025
pp. 587–600

Research paper

Experimental study on interaction characteristics of geogrid-clay interface

Wei Fu[1], Ke Liu[2], XiangPing Li[3]

Abstract: Geogrid is a kind of geosynthetic material widely used in engineering. The interaction between geogrid and packed soil plays a decisive role in the stability of reinforced soil engineering. In this paper, the influence of normal stress, type of geogrid, water content and compactness of subgrade soil on the effect of reinforcement was studied, and the influence degree of each factor was analyzed by grey correlation method. The results show that under the same conditions, both the friction-like coefficient and the maximum shear stress of reinforced soil with bi-directional geogrid are significantly higher than those with unidirectional geogrid. With the increase of normal stress, the maximum shear stress between reinforcement and soil increases, while the friction coefficient decreases slightly with the increase of normal stress. The higher the compactness of the filler, the higher the friction coefficient between the reinforcement and soil. The higher the moisture content, the smaller the friction coefficient between the soil and the reinforcement. According to the grey correlation method, the influence of each factor from large to small is type of geogrid > degree of compaction > water content > normal stress. Therefore, it is suggested that bidirectional grid should be used in engineering and reduce the water content appropriately, which will make the geogrid reinforcement effect reach the best. An elastic-exponential hardening model was proposed to describe and analyze the interface behavior of bidirectional geogrid reinforced clay, and the results can be used as a guide for clay stiffening engineering.

Keywords: geogrid, clay, pull-out test, interface action characteristics

[1]Eng., Second Highway Survey, Design and Research Institute, Wuhan, 430056, China, e-mail: 19632003@qq.com, ORCID: 0009-0002-5317-9668

[2]M. Eng., Changsha University of Science and Technology, School of Transportation Engineering, Changsha, 410000, China, e-mail: liuke@stu.csust.edu.cn, ORCID: 0009-0004-3661-7894

[3]S. Eng., Shenzhen Urban Traffic Planning and Design Research Center, Shenzhen, 518000, China, e-mail: lxpc-sust@163.com, ORCID: 0000-0002-3172-9588

1. Introduction

Geogrids are characterized by their low cost and convenient installation. When geogrids are placed in soil, they utilize the frictional interaction between the geogrids and the soil to effectively resist tensile forces and compressive stresses resulting from soil deformation. The interaction between geogrids and fill materials is a key factor in describing the reinforcement mechanism. The interaction between soil and geogrids is an important consideration in the analysis and design of geogrid-reinforced structures, commonly used in engineering applications such as retaining walls, soft soil foundations, steep slopes, and roads [1].

Many researchers have conducted laboratory pull-out tests to investigate the effects of geogrid types, fill materials, and test conditions. The effect of moisture content on the pull-out behavior of unidirectional geogrids in cohesive clay and found that the ultimate pull-out force decreases with increasing moisture content [2, 3]. Indoor pull-out tests on geogrids with different proportions of transverse and longitudinal ribs in sand found that the tensile modulus and grid stiffness are important influencing factors on pull-out force [4, 5]. The increase in pull-out force by transverse ribs exceeded 2/3 of the total increment. At higher pull-out rates, the interface strength between the geogrid and soil increases, resulting in uneven distribution of normal stresses and a decrease in interfacial frictional resistance [6]. Pull-out tests under dynamic and static loads to investigate the effects of normal stress, amplitude, and frequency on the geogrid-soil interface behavior [7]. The results showed that the pull-out force exhibits different growth patterns with increasing normal stress. Additionally, the compaction degree of the fill material significantly affects the interlocking force between the fill material and geogrid, highlighting the importance of fill compaction on the reinforcement effect.

This study conducted pull-out tests to experimentally investigate the interface behavior of geogrid-reinforced clay while controlling variables such as normal stress, geogrid type, fill material moisture content, and fill compaction degree. The grey correlation method was employed to determine the degree of influence of each variable. Furthermore, a segmented elastic-exponential hardening model was proposed and verified to provide a better fit for describing the behavior of the geogrid-soil interface in pull-out tests.

2. Test materials and test equipment

2.1. Test materials

The experiment utilized low liquid limit clay as the fill material. The basic performance parameters of the soil are presented in Table 1. The grading curve was shown in Fig. 1.

Table 1. Basic performance parameters of soil

Type of filler	Liquid limit (%)	Plastic limit (%)	Plasticity index (%)	Maximum dry density (g/cm^3)	Optimum moisture content (%)
Clay	39.2	21.4	17.8	1.84	21.4

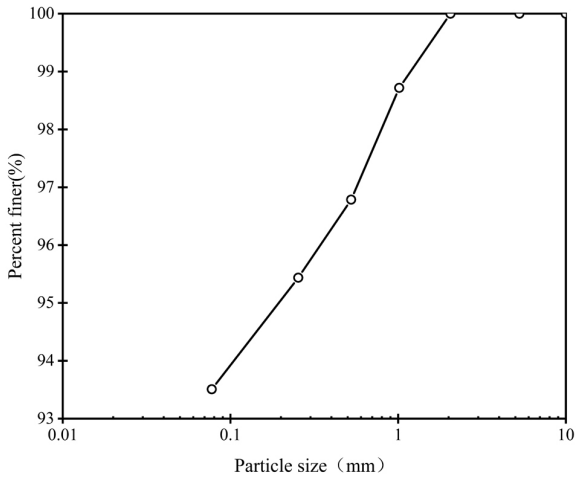

Fig. 1. Gradation curve of soil

The geogrids selected for the experiment are commonly used in highway subgrade reinforcement: a bidirectional plastic geogrid (TGSG 50) and a high-density polyethylene uniaxial geogrid (HDPE). For experimental convenience, the bidirectional geogrid was cut into rectangular pieces measuring approximately 350 × 110 mm. The parameters of the geogrids are presented in Table 2. The geogrid was shown in Fig. 2.

Table 2. Parameters of geogrid for test

Grille type	**Tensile strength (kN/m)**		
	Yield strength per meter of longitudinal tension	**Tensile force at 2% elongation**	**Tensile force at 5% elongation**
TSGS	50	17.5	35
HDPE	200	70	110

Fig. 2. Geogrid for testing

2.2. Test equipment

This experiment utilizes the YT1200S direct shear-pull friction tester for geosynthetic reinforcement of soil, manufactured by Wenzhou Jingai Instrument Co., Ltd., referred to as the "pullout tester". The device, shown in Fig. 3, is employed to conduct the experiment.

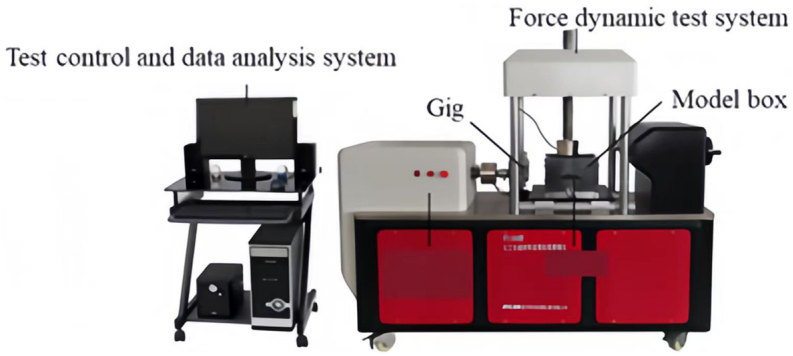

Fig. 3. YT 1200 S Geosynthetic material direct shear drawing friction instrument

2.3. Test scheme

Based on the results of the basic performance tests of the subgrade soil and the actual engineering conditions, a simulation is carried out to evaluate the stress distribution of geogrids in the subgrade during highway operation. The geogrid experiences an upper load of approximately 40 kPa when placed in the middle of the roadbed, 60 kPa in the middle of the subgrade, and 80 kPa at the bottom. Thus, for this experiment, normal stresses of 40 kPa, 60 kPa, and 80 kPa are selected. Regarding the selection of moisture content, it ranges from 0.8 times the Optimum Moisture Content (OMC) to 1.2 times the OMC, covering the actual moisture content of the subgrade soil in engineering projects. According to the "Highway Subgrade Design Specifications" in China (JTG D 30-2015), the compaction degree on the upper and lower roadbeds should be equal to or greater than 94%, and for expressways and first-grade highways, it should be equal to or greater than 96%. The compaction degree on the upper road embankment should be equal to or greater than 93%, while on the lower road embankment, it should be equal to or greater than 90%, and the compaction degree on the sub-base should not be less than 90%. The compaction degree of older road subgrades mainly ranges from 85% to 95%. Therefore, considering the actual engineering conditions, this experiment selects compaction degrees of 85%, 90%, and 95% for the fill materials.

To investigate the influence of various factors on the pullout test and improve the accuracy of the experiment, single-factor pullout tests are designed for factors such as normal stress, fill material compaction degree, fill material moisture content, and geogrid type. Each test is conducted in triplicate, and the average value is calculated after excluding outliers, resulting in a total of 42 experiments.

Table 3. Drawing test design table

Test	Normal stress (kPa)	Filler water content (%)	Filler compaction degree (%)	Grid type
1	40	OMC	90	Unidirectional
2	60	OMC	90	
3	80	OMC	90	
4	60	0.8 OMC	90	
5	60	1.2 OMC	90	
6	60	OMC	85	
7	60	OMC	95	
8	40	OMC	90	Bidirectional
9	60	OMC	90	
10	80	OMC	90	
11	60	0.8 OMC	90	
12	60	1.2 OMC	90	
13	60	OMC	85	
14	60	OMC	95	

3. Experimental results and data analysis

3.1. Experimental results

Considering that the interface strength between geogrid and soil is primarily governed by the interlocking effect of the transverse ribs, using apparent friction angle and apparent cohesion to reflect the interface strength does not fully adhere to the frictional behavior [8]. In this study, we draw inspiration from the methods presented in references [8] and [9] and introduce a coefficient of apparent friction f at the geogrid-soil interface. This coefficient effectively accounts for the interlocking effect between the geogrid and soil and takes advantage of the automatic determination of maximum shear stress provided by the testing apparatus. The calculation formula is as follows:

$$\tau_p = \frac{Td}{2LB} \tag{3.1}$$

$$f = \frac{\tau_{\max}}{\sigma_n} = \tan \varphi_{sg}^* \tag{3.2}$$

where: T_d – peak horizontal drawing force or horizontal drawing force when pulling out, kN; L, B – length and width of the geoglass embedded in the filler, m; τ_p – maximum friction strength at the stiff-soil interface, kPa; σ_n – normal stress, kPa; φ_{sg}^* – combined friction angle (°). The contribution of interlocking between reinforcement and soil to the interfacial strength of reinforcement and soil is considered.

Incorporating equation (3.1) and equation (3.2), the experimental results obtained under various variable conditions are shown in the table below:

Table 4. Pull-out test results

Test	Normal stress (kPa)	Filler water content (%)	Filler compaction degree (%)	Grid type	Shearing stress (kPa)	Coefficient of apparent friction
1	40	OMC	90	Unidirectional	36.8	0.92
2	60	OMC	90		50.3	0.84
3	80	OMC	90		58.4	0.73
4	60	0.8OMC	90		60.5	1.01
5	60	1.2OMC	90		36.9	0.62
6	60	OMC	85		44.1	0.74
7	60	OMC	95		54.8	0.91
8	40	OMC	90	Bidirectional	67.6	1.69
9	60	OMC	90		93.7	1.56
10	80	OMC	90		113.6	1.42
11	60	0.8OMC	90		100.4	1.67
12	60	1.2OMC	90		82.8	1.38
13	60	OMC	85		84.5	1.41
14	60	OMC	95		101.0	1.68

3.2. Effect of normal stress on the interface characteristics of reinforcement and soil

From the experimental results shown in Fig. 4, it can be observed that even when the uniaxial geogrid has a higher strength compared to the biaxial geogrid, the biaxial geogrid exhibits a significant increase in both the coefficient of apparent friction and the maximum shear stress. This can be attributed to the presence of transverse ribs, which enhances the interlocking effect between the geogrid and the soil. As the normal stress increases, the maximum shear stress at the interface also increases, indicating that the interface coefficient of apparent friction and shear stress are greater in the vicinity of the lower part of the roadbed where the geogrid is placed. This highlights the enhanced reinforcement effect. The findings further support the results obtained by other researchers through numerical simulations and model tests [10]. The coefficient of apparent friction slightly decreases with an increase in normal stress. This can be explained by equation (3.2), which shows that as the normal stress increases, the increase in shear stress between the geogrid and soil is not as significant as the increase in normal stress. Additionally, as the normal stress increases, it is possible that the geogrid is not fully engaged throughout its length, leading to a decrease in the coefficient of apparent friction at the interface.

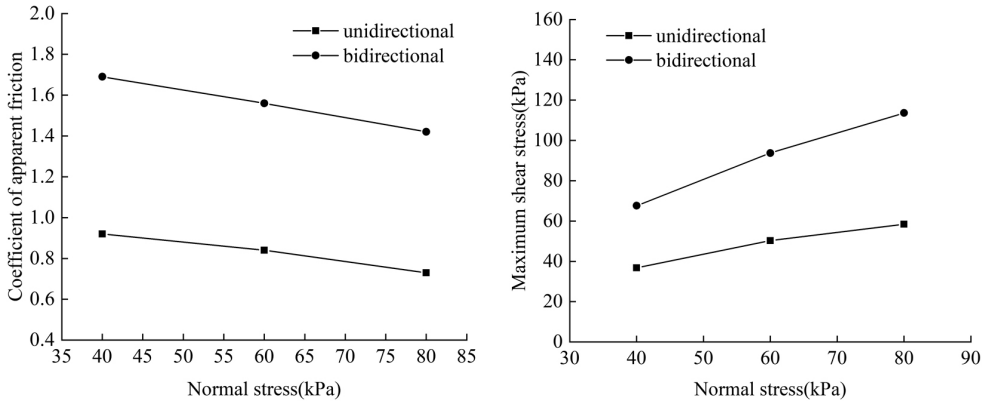

Fig. 4. Friction similarity coefficient and maximum shear stress under different normal stresses: (a) Coefficient of apparent friction, (b) Maximum shear stress

3.3. Effect of filler moisture content and filler compaction degree on the characteristics of stiff-soil interface

Analysis of Fig. 5 reveals that as the water content increases, the coefficient of apparent friction between the geogrid and soil gradually decreases. The higher the water content, the greater the decrease in the coefficient of apparent friction. This can be attributed to the presence of excess water, which creates a smoother interface between the geogrid and soil. Moreover, when the water content is excessively high, the backfill material becomes loose, leading to a reduction in the coefficient of apparent friction at the interface. Based on this observation,

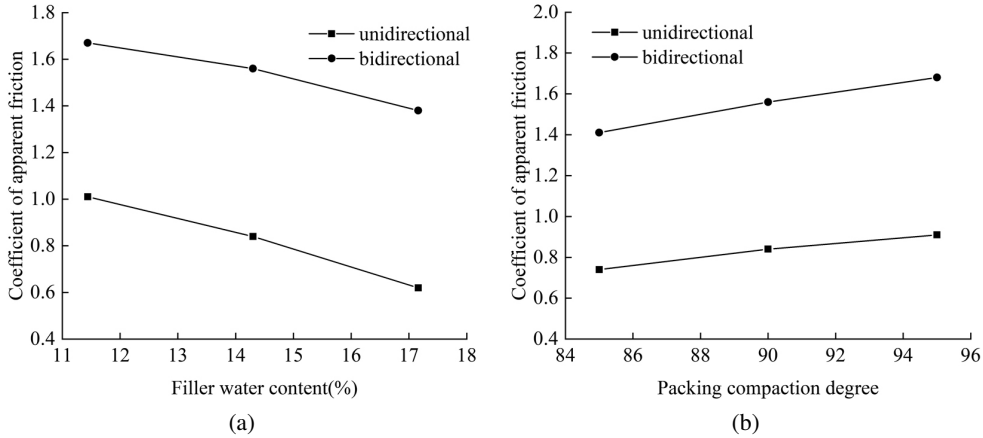

Fig. 5. The coefficient of apparent friction of packing under different water content and compactness: (a) Filler water content, (b) Filler compaction degree

it can be inferred that if the water content continues to increase, the compaction degree will decrease, subsequently resulting in both the apparent cohesion and the peak pullout force of the fill material becoming zero [11]. Conversely, as the compaction degree of the fill material increases, the coefficient of apparent friction also increases. Therefore, to enhance the reinforcement effect during construction, it is crucial to strictly control the water content of the fill material. Additionally, supplemental compaction or dynamic compaction can be employed to improve the compactness of the embankment.

3.4. Analysis of the influence degree of each influencing factor on the stiff-soil interface characteristics

To determine the key factors affecting the coefficient of apparent friction f at the geogrid-soil interface, a grey relational analysis was conducted in this experiment. In this analysis, the coefficient of apparent friction $X_0 = \{x_0(k),\ k = 1, 2, \ldots, n\}$ was taken as the reference sequence, while the normal stress, fill material water content, fill material compaction degree, and geogrid type $X_i = \{x_i(k),\ k = 1, 2, \ldots, n\}$ were taken as the comparative sequences. To facilitate the analysis, a mean normalization technique was applied to the factors. The geogrid type was handled by assigning the values 1 and 2 to uniaxial and biaxial geogrids, respectively, based on the influence of transverse ribs. The transformed results are presented in Table 5.

Table 5. Initial value transformation result

X_1	X_2	X_3	X_4	X_0
0.6667	1	1	0.6667	0.7768
1	1	1	0.6667	0.7093
1.3333	1	1	0.6667	0.6164
1	0.8	1	0.6667	0.8528
1	1.2	1	0.6667	0.5235
1	1	0.9444	0.6667	0.6248
1	1	1.0556	0.6667	0.7684
0.6667	1	1	1.3333	1.427
1	1	1	1.3333	1.3172
1.3333	1	1	1.3333	1.199
1	0.8	1	1.3333	1.4101
1	1.2	1	1.3333	1.1653
1	1	0.9444	1.3333	1.1906
1	1	1.0556	1.3333	1.4186

In order to determine the degree of correlation between the comparative sequence and the reference sequence, the discrete function of the correlation coefficient, known as the grey relational coefficient, can be obtained using the following equation:

$$\xi_i(k) = \frac{\min_i \min_k |X_i(k) - X_0(k)| + \rho \max_i \max_k |X_i(k) - X_0(k)|}{|X_i(k) - X_0(k)| + \rho \max_i \max_k |X_i(k) - X_0(k)|} \tag{3.3}$$

$$\Delta_{\max} = \max_i \max_k \{\Delta_{0i}(k)\} (i = 1, 2, \ldots, m;\ k = 1, 2, \ldots n) \tag{3.4}$$

$$\Delta_{\min} = \min_i \min_k \{\Delta_{0i}(k)\} (i = 1, 2, \ldots, m;\ k = 1, 2, \ldots n) \tag{3.5}$$

where: $\Delta_{\max}$ and $\Delta_{\min}$ represent the maximum and minimum absolute differences, respectively; ρ represents the distinguishing coefficient, which generally takes values between 0 and 1. In this article, it is set to 0.5 [12]. To calculate the absolute difference between the reference sequence and other factors, the equation (3.6) can be used. The results are shown in Table 6.

$$\Delta_i k = |X_i(k) - X_0(k)| \tag{3.6}$$

Table 6. Table of absolute differences

X_1	X_2	X_3	X_4
0.1102	0.2232	0.2232	0.1102
0.2907	0.2907	0.2907	0.0426
0.7169	0.3836	0.3836	0.0503
0.1472	0.0528	0.1472	0.1862
0.4765	0.6765	0.4765	0.1431
0.3752	0.3752	0.3196	0.0418
0.2316	0.2316	0.2872	0.1017
0.7604	0.4270	0.4270	0.0937
0.3172	0.3172	0.3172	0.0161
0.1343	0.1990	0.1990	0.1343
0.4101	0.6101	0.4101	0.0768
0.1653	0.0347	0.1653	0.1681
0.1906	0.1906	0.2461	0.1427
0.4186	0.4186	0.3630	0.0852

To calculate the grey relational degree for each curve

$$r_i = \frac{1}{n} \sum_{k=1}^{n} \xi_i(k) \tag{3.7}$$

According to equation (3.7), the calculated results are as follows: $r_1 = 0.56539$; $r_2 = 0.58370$; $r_3 = 0.56724$; $r_4 = 0.8011$. Therefore, under lower normal stress, the significance of various factors in influencing the results is as follows: geogrid type > fill water content > fill compaction degree > normal stress.

3.5. Shear stress-displacement diagram analysis

Figure 6 presents the shear stress-displacement curves under different conditions. According to Fig. 5, it can be observed that at smaller horizontal displacements, the shear stress between the single and double geogrid interfaces increases linearly with increasing horizontal displacement. As the horizontal displacement further increases, the shear stress

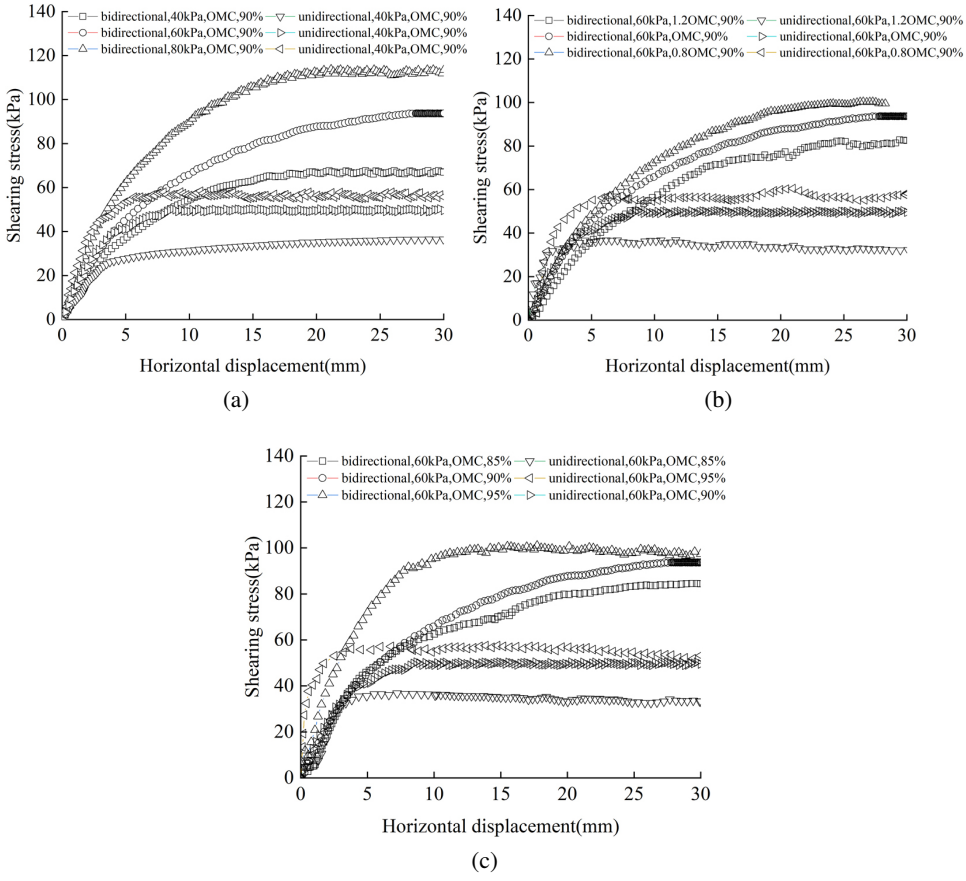

Fig. 6. Shear stress displacement diagram: (a) Shear stress-displacement diagram under different normal stresses, (b) Shear stress-displacement diagram with different water content, (c) Shear stress-displacement diagram under different compactness

exhibits a nonlinear increase and eventually reaches a steady value. The shear stress of the single geogrid reaches its peak quickly after the linear increase, while the shear stress of the double geogrid undergoes a relatively longer period of nonlinear growth. The possible reason for this difference is that the double geogrid is placed within the soil, and when relative sliding occurs between the geogrid and the soil, the soil undergoes a gradual densification process due to the interlocking effect of the ribs with the soil. Additionally, as the normal stress increases, the slope of the shear stress curve becomes steeper during the linear increase.

The process of geogrid pullout is a progressive failure process, which can be characterized by two types of curves: strain hardening and strain softening. For single geogrid reinforcement, the pullout curve exhibits a strain softening behavior. Due to the interlocking effect between the ribs and the fill, the pullout curve of the double geogrid generally shows a strain hardening behavior, which gradually changes from strain hardening to strain softening with an increase in the rib spacing [12, 13]. In this experiment, due to limitations of the testing apparatus, the pullout displacement was limited. As a result, the strain softening behavior was not observed in the pullout test of the single geogrid. Therefore, this analysis is focused on the pullout behavior of the double geogrid interface.

The shear stress-displacement curve of the strain-hardening geogrid-soil interface, as shown in Fig. 7, exhibits distinct stages during the pullout test. In the initial stage (Stage I), when the displacement is small, the geogrid is in its elastic state. At this stage, the interface shear stress shows a linear relationship with shear displacement. As the pullout force and displacement gradually increase, the geogrid near the pullout end enters the plastic state first (Stage II) and continues to extend towards the burial end. There exists a critical point P between the elastic and plastic state regions. Once the plastic state is reached (Stage III), the shear stress no longer changes. When the geogrid is completely in the plastic state, the interface shear stress between the reinforcement and the soil will remain constant and no longer vary.

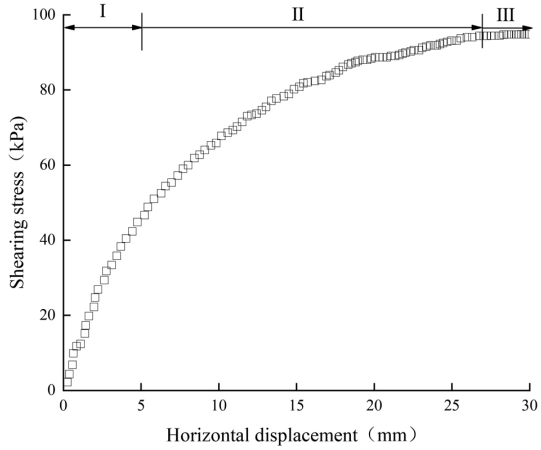

Fig. 7. Schematic diagram of each stage of strain hardening type

3.6. An applicable model for the interface description of reinforcement and soil in drawing test

When the pullout curve exhibits strain hardening behavior, it is generally assumed that the geogrid-soil interface undergoes three stages: pure elasticity, elastic-plastic, and fully plastic, under the action of loads during the pullout test. To simplify the complex process in the pullout test, many researchers have adopted ideal elastic-plastic models [14] and bilinear models [15] to describe and analyze the behavior characteristics of the geogrid-soil interface. The relationships expressed by equations (3.8) and (3.9) are used for this purpose.

$$\tau = \begin{cases} kul & 0 \le u \le u_1 \\ \tau_{\max} & u_1 < u \end{cases} \tag{3.8}$$

$$\tau = \begin{cases} k_1 u & 0 \le u \le u_1 \\ k_2 u & u_1 \le u \end{cases} \tag{3.9}$$

However, both of these classic models are linear models, leading to significant errors when compared to the actual shear stress between the reinforcement and soil during experimental procedures, and they cannot capture the nonlinearity of the geogrid-soil interface. In this study, the shear stress-displacement curve is simplified using an elastic-exponential hardening model, and the pullout test is divided into two stages. The relationship expression is given as equation (3.10):

$$\tau = \begin{cases} ku & 0 \le u \le u_1 \\ \tau_{\max}(1 - e^{\xi u}) & u_1 < u \end{cases} \tag{3.10}$$

where k is defined as the linear growth coefficient during the linear stage, which is related to the performance parameters of geogrid, fill condition, etc. $\tau_{\max}$ represents the maximum shear stress during the pullout test, u_1 represents the shear displacement at the end of the pure elastic stage, and ξ is defined as the geogrid plastic decay coefficient.

This paper selects the pullout test data under the conditions of 60 kPa, optimal moisture content, and 90% compaction degree to compare the fitting effects of various models. The fitting results of each model are shown in Fig. 8.

From the figure, it can be observed that when using the ideal elastic-plastic model to describe the interface pullout behavior, the interface shear stress is overestimated in both the elastic (Stage I) and elastic-plastic stages (Stage II). As for the bilinear model, the interface shear stress is higher than the actual shear stress in the elastic stage, but becomes lower in the later stage of elastic-plastic behavior. Comparatively, the elastic-exponential model shows the best fitting effect, closely matching the experimental results. Therefore, this segmented elastic-exponential hardening model is more suitable for describing and analyzing the interface behavior of bi-directional geogrid-reinforced soil.

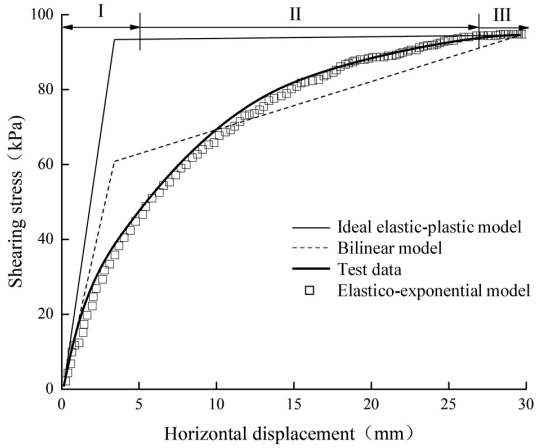

Fig. 8. Determine the corresponding shear stress at point P under each working condition

4. Conclusions

1. The presence of transverse ribs in bi-directional geogrids increases the interlocking effect between the reinforcement and soil, leading to significant increases in apparent friction coefficient and maximum shear stress compared to uni-directional geogrids. The interface shear stress between the reinforcement and soil increases linearly with normal stress, while the apparent friction coefficient decreases with increasing normal stress. The apparent friction coefficient increases with increasing fill compaction degree and decreases with increasing fill moisture content, with a greater decrease at higher moisture content.
2. The analysis of the significant factors affecting the apparent friction coefficient at the reinforcement-soil interface shows that the factors are ranked in the following order: geogrid type > fill compaction degree > fill moisture content > normal stress.
3. Based on the analysis of the shear stress-displacement curve of the test, the pullout test process is divided into a linearly rising elastic stage, a non-linearly rising elastic-plastic stage, and a plastic stage where the shear stress tends to a constant value. Due to the gradual densification process between the transverse ribs and the soil, the elastic-plastic rising stage is longer. It is proposed to use a segmented elastic-exponential hardening model to describe and analyze the interface behavior, which has been validated to have good fitting effects and is more suitable for describing and analyzing the interface behavior in pullout tests of geogrid-reinforced soil.

Acknowledgements

Fund project: 1. Supported by National Key Research and Development Program (Project number: 2021YFB2600900). 2. China Communications Construction Group Youth Science and Technology Innovation Project (2021-ZJKJ-QNCX16)

References

[1] L. Hoe, A. Pamuk, M. Dechasakulsom, Y. Mohri, and C. Burke, "Interaction between PVC geomembranes and compacted clays", *Journal of Geotechnical and Geoenvironmental Engineering*, vol. 127, no. 11, pp. 950–954, 2001, doi: 10.1061/(ASCE)1090-0241(2001)127:11(950).

[2] F. Xiaojing, Y. Qing,and L. Shoulong, "Pullout Behavior of Geogrid in Red Clay and the Prediction of Ultimate Resistance", *Electronic Journal of Geotechnical Engineering*, vol. 13, pp. 101–117, 2008.

[3] F. Haynes, C. Collins, and W. Olson, *Bearing capacity tests on ice reinforced with geogrids*. The American Society of Mechanical Engineers, 1992.

[4] A. Abdel-Rahman, "Modeling of soil-geosynthetic interaction in reinforced earth works, PhD dissertation, New Orleans, Tulane University, 1997.

[5] N. Moraci and D. Gioffrè, "A simple method to evaluate the pullout resistance of extruded geogrids embedded in a compacted granular soil", *Geotextiles and Geomembranes*, vol. 24, no. 2, pp. 116–118, 2005, doi: 10.1016/j.geotexmem.2005.11.001.

[6] A. Pant, G. Ramana, M. Datta, and S. Gupta, "Coal combustion residue as structural fill material for reinforced soil structures", *Journal of Cleaner Production*, vol. 232, pp. 417–426, 2019, doi: 10.1016/j.jclepro.2019.05.354.

[7] Z. Zuo, G. Yang, H. Wang, and Z. Wang, "Experimental Investigations on Pullout Behavior of HDPE Geogrid under Static and Dynamic Loading", *Advances in Materials Science and Engineering*, vol. 2020, no. 7, pp. 1–13, 2020, doi:10.1155/2020/5408064.

[8] C. Chen, G. McDowell, and N. Thom, "A study of geogrid-reinforced ballast using laboratory pull-out tests and discrete element modeling", *Geomechanics and Geoengineering*, vol. 8, no. 4, pp. 244–253, 2013, doi:10.1080/17486025.2013.805253.

[9] Y. Dong, J. Han, and X. Bai, "Numerical analysis of tensile behavior of geogrids with rectangular and triangular apertures", *Geotextiles and Geomembranes*, vol. 29, no. 2, pp. 83–91, 2011, doi: 10.1016/j.geotexmem.2010.10.007.

[10] A. Mirzaalimohammadi, M. Ghazavi, M. Roustaei, and S. Lajevardi, "Pullout response of strengthened geosynthetic interacting with fine sand", *Geotextiles and Geomembranes*, vol. 47, no. 4, pp. 530–541, 2019, doi: 10.1016/j.geotexmem.2019.02.006.

[11] Z. Junhui, Z. Anshun, L. Jue, L. Feng, and P. Junhui, "Gray Correlation Analysis and Prediction on Permanent Deformation of Subgrade Filled with Construction and Demolition Materials", *Materials*, vol. 12, no. 18, 2019, doi: 10.3390/ma12183035.

[12] C. Jianhang, S. Saydam, and C. Hagan, "An analytical model of the load transfer behavior of fully grouted cable bolts", *Construction and Building Materials*, vol. 101, pp. 1006–1016, 2015, doi: 10.1016/j.conbuildmat.2015.10.099.

[13] Z. Jianjun and D. Jianguo, "Prediction of the nonlinear pull-out response of FRP ground anchors using an analytical transfer matrix method", *Engineering Structures*, vol. 81, pp. 377–385, 2014, doi: 10.1016/j.engstruct.2014.10.008.

[14] Z. Honghu, Z. Chenchen, T. Chaosheng, S. Bin, and W. Baojun, "Modeling the pullout behavior of short fiber in reinforced soil", *Geotextiles & Geomembranes*, vol. 42, no. 4, pp. 329–338, 2014, doi: 10.1016/j.geotexmem.2014.05.005.

[15] G. Alfano and E. Sacco, "Combining interface damage and friction in a cohesive-zone model", *International Journal for Numerical Methods in Engineering*, vol. 68, no. 5, pp. 542–582, 2006, doi: 10.1002/nme.1728.

Received: 2023-11-12, Revised: 2024-03-14